

AN ABSTRACT OF THE THESIS OF

Robert D. Govier for the degree of Master of Science in
Chemistry presented on December 10, 1992.

Title: ESCA Studies of a Brass Surface Subjected to Gas-Jet
Enhanced Sputtering

Redacted for privacy

Abstract approved: _____

Edward H. Piepmeier

The inert gas ion bombardment of solid surfaces has found many uses in the field of analytical chemistry. In one method of spectrochemical analysis, inert gas ion bombardment in a glow discharge is used to produce an atomic vapor, representative of the sample bulk, which is analyzed using atomic absorption techniques. Gas jets directed at the sample surface during the discharge increase the removal rate of sample material from the surface. Such bombardment of solid surfaces results in changes to the surface which are visually evident in the formation of craters and surface deposits. This thesis was designed to gain a better understanding of the changes in a brass surface caused by jet-enhanced sputtering. Electron spectroscopy for chemical analysis (ESCA) is used to study selected regions of the surface. Changes in chemical composition were observed as successive atomic layers were removed from the sample.

The results of this investigation indicate that the

effects of ion bombardment can be explained in terms of the selective sputtering of one bulk component over another. The surfaces of the sputtered craters were found to be depleted of the higher sputtering yield component, Zn, when compared to the bulk composition. In a deposit, the component with the highest sputtering yield was found to be more concentrated in layers closest to the bulk material. The component with the lowest sputtering yield was found at relatively higher concentrations nearest the deposit surface. The component with the higher sputtering yield is selectively sputtered first during the glow discharge, and consequently is deposited with a higher concentration closest to the bulk, the converse being true for the lowest sputtering yield component.

ESCA Studies of a Brass Surface Subjected to
Gas-Jet Enhanced Sputtering

by

Robert D. Govier

A THESIS

submitted to

Oregon State University

in partial fulfillment of
the requirements for the
degree of

Master of Science

Completed December 10, 1992

Commencement June 1993

APPROVED

Redacted for privacy

Professor of Chemistry in charge of major _____

Redacted for privacy

Head of department of Chemistry _____

Redacted for privacy

Dean of Graduate School _____

Date thesis is presented December 10, 1992

Typed by Robert D. Govier

ACKNOWLEDGEMENT

I wish to thank the many individuals and organizations which have supported me in the completion of this thesis. The U. S. Bureau of Mines, Albany Research Center, provided the financial support, the ESCA and many of the other necessities required to perform the analyses. Oregon State University provided the glow discharge cell and other equipment necessary to prepare the sample for analysis. I wish to thank Dr. E. H. Piepmeier of OSU for his advice and patience and Ms. Jane Knoper, formerly of the Bureau of Mines, for the advice and instruction she provided in the operation of the ESCA. Last, but most of all, I wish to thank my family for the patience and moral support that they have provided during the time that I have been at OSU.

TABLE OF CONTENTS

INTRODUCTION	1
THEORY	3
EXPERIMENTAL	8
RESULTS AND DISCUSSION	16
Bulk Materials	16
Surface Deposits	25
Crater Areas	33
CONCLUSIONS	41
BIBLIOGRAPHY	43
APPENDIX	44

LIST OF FIGURES

<u>Figure</u>		Page
1.	Side view schematic of gas-jet enhanced sputtering atomizer	9
2.	Locations where depth profile data were collected	10
3.	Examples of spectral peaks (binding energy vs. counts) collected at location C after 40 s etch time	12
4.	Calculated atomic ratios for locations A and F	17
5.	Measured binding energies at location A	21
6.	Measured binding energies at location F	22
7.	Calculated atomic ratios and measured binding energies at location B	26
8.	Calculated atomic ratios and measured binding energies at location C	27
9.	Calculated atomic ratios and measured binding energies at location E	28
10	Cross sectional diagram indicating the changes to the sample surface resulting from gas-jet enhanced sputtering by the Atomsources	32
11.	Calculated atomic ratios and measured binding energies at location G	34
12.	Calculated atomic ratios and measured binding energies at location H	35
13.	Calculated atomic ratios and measured binding energies at location D	36

ESCA STUDIES OF A BRASS SURFACE SUBJECTED
TO GAS-JET ENHANCED SPUTTERING

INTRODUCTION

The use of inert gas ion bombardment of solid surfaces has had application in analytical chemistry for many years. Hollow cathode lamps are used in atomic absorption spectrometry as a line source in the determination of many elements. Metals and solution residues have been analyzed using ion bombardment as a source of sample atoms⁽¹⁾. Currently, at least one instrument is commercially available which uses inert gas ion bombardment of samples to produce an atomic vapor which is then analyzed by atomic absorption spectrometry⁽²⁾.

Physical and chemical phenomena associated with the inert gas ion bombardment of surfaces have been studied experimentally for decades. Such basic information as sputtering yields of pure elements have been determined by many authors^(3,4,5), and attempts have been made to understand the sputtering yields of materials on a theoretical basis^(6,7). Surface morphology resulting from sputtering has been studied using the scanning electron microscope (SEM) in order to better understand sputtering effects when sputtering is used as an analytical tool^(1,2,8).

The effects of inert gas ion bombardment on surfaces have been studied using electron spectroscopy for chemical

analysis (ESCA)⁽⁹⁾. In this technique photoelectrons, which are emitted by the sample upon exposure to X-rays, are analyzed. Photoelectrons of energies encountered in ESCA analysis are only able to escape from depths within the sample which correspond to several atomic layers. ESCA, therefore, is a technique that provides information about the topmost atomic layers of the surface of a sample. One of the most common variants of this analytical technique uses inert gas ion beams to etch away layers of atoms from the sample surface, thereby exposing successive atomic layers for analysis⁽¹⁰⁾.

This thesis describes work which was done using ESCA to characterize the various morphologies present on a brass surface after it was subject to inert gas ion bombardment in the presence of gas jets. The ion bombardment (sputtering) was done under conditions similar to those encountered when ion bombardment is used to produce an atomic vapor for atomic absorption analysis. These conditions were chosen in attempts to develop a better understanding of the sputtering processes in the presence of gas jets, and to explore the effects that such sputtering has on sample surfaces.

THEORY

In an ESCA experiment X-rays of known energy are directed at the sample resulting in emission of photoelectrons. These photoelectrons are emitted with a kinetic energy that is equal to the energy of the incident X-rays minus the photoelectron binding energy, that is, the energy required to remove those electrons from their atomic orbits. By measuring the kinetic energy of the photoelectrons one can use the simple relationship mentioned above to calculate their binding energy in the sample. Binding energy data are useful because they are an indication of electronic environment and hence chemical state. Binding energy data can be interpreted in the light of the charge-potential model of the atom⁽¹¹⁾.

According to this model, the atom is regarded as a hollow sphere upon which the valence electron charge resides. The potential, then, inside the sphere is the same at all points. A change in valence electron density results in a change in the potential at all points within the sphere. Therefore, the binding energy of all core electron energy levels changes by the same amount. A decrease in valence electron density causes an increase in binding energy. In other words, as the electronegativity of neighboring atoms increases, the binding energy of the atoms in question also increases. Conversely, as more of the electronegative species present in the sample are removed, the binding energy of the remaining atoms should decrease.

The experimental observations made during the course of this present work correlate well with theory. Specifically, as the oxygen content of the sample decreased, the electronic binding energy of the remaining oxygen, zinc and copper also decreased.

In addition to binding energy, photoelectron current (intensity) is also recorded. The photoelectron intensity, arising from a specific electronic shell of an atomic species, is related to the volume density of the atoms of that species. The relationship between the volume density of a particular atomic species and the photoelectron intensity has been developed from first principles by Powell⁽¹²⁾. His equations were adapted for use in this present work so that ratios of the numbers of atoms of a species could be reported rather than the volume density of a particular species. For example, rather than report the volume densities of Cu, Zn and O, the atomic ratios Zn/Cu and O/Cu are reported. Reporting of atomic ratios allows for simplified mathematics and more accurate quantitative values while providing enough information so that substantive conclusions can be drawn. Powell's equation relating photoelectron intensity and volume density of the *i*th species is:

$$I_i = I_0 N_i \sigma_i \lambda_i F_i T_i D_i G$$

where

I_i = measured photoelectron intensity from
a specific shell of atomic species *i*

I_0 = incident X-ray flux

N_i = volume density of atoms of species i

σ_i = differential photoionization cross section for the specific shell of the atomic species i at the characteristic energy of the X-ray beam

λ_i = inelastic mean free path in the sample of photoelectrons emitted from a specific shell of atoms of species i

F_i, T_i, D_i = factors which describe various aspects of the instrument response function for photoelectrons emitted from species i

G = geometric factor which describes the solid angle of collection of the photoelectrons and the area of the sample irradiated by the incident X-ray beam

For two different atomic species i and j ,

$$\frac{I_i}{I_j} = \frac{I_0 N_i \sigma_i \lambda_i F_i T_i D_i G}{I_0 N_j \sigma_j \lambda_j F_j T_j D_j G}$$

Combining the factors F , T and D into a single instrument response function R for each atomic species present, cancelling like terms and rearranging gives:

$$\frac{N_i}{N_j} = \frac{I_i \sigma_j \lambda_j R_j}{I_j \sigma_i \lambda_i R_i}$$

Note that it no longer becomes necessary to know the values of the incident X-ray flux or the geometric factor, quantities which might be difficult to obtain. In the present experiments atomic ratios were calculated from measured intensity ratios. The value of the quantity

$$\frac{\sigma_j \lambda_j R_j}{\sigma_i \lambda_i R_i}$$

has been treated as a constant. The reason that this quantity can be regarded as a constant is explained as follows.

Differential photoionization cross section (σ) values have been calculated by Schofield for the elements from atomic number 1 to 96. These values are presented in tabular form in reference 13. Ratios are constant for a single excitation source and are easily calculated.

The instrument response function (R) is a quantity which depends on the energy of the photoelectrons being measured. The values of the instrument response functions for Zn and Cu were measured using the pure elements. The ratio of the instrument response functions, R_{Zn}/R_{Cu} , was calculated from these measured values. The instrument response function ratio R_o/R_{Cu} was measured using the compound CuO. If measurement of sample photoelectron intensity is made under the same conditions as that of the

pure elements and CuO, then the instrument response function ratio can be regarded as a constant for the element pairs, Zn/Cu and O/Cu.

The inelastic mean free path of photoelectrons in the sample (λ) is a variable whose value depends on both photoelectron energy and sample composition. Tanuma et. al.⁽¹⁴⁾ have given a method to calculate the value of λ for materials. However, the very information which is sought in this experiment, sample composition, is required to accomplish the calculation. If atomic ratio information is sufficient to draw substantive conclusions about the sample, then the situation is greatly simplified. The simplification arises because the calculation of atomic ratios requires the knowledge only of the ratio of the inelastic mean free paths. This ratio remains virtually constant in spite of widely varying composition. Therefore the ratio can be calculated for one composition and used in all atomic ratio calculations. The fact that the ratio of the inelastic mean free paths remains constant is demonstrated in the appendix where the ratio is calculated for some of the extremes of composition expected.

EXPERIMENTAL

Solid brass spectrographic standard #NBS 1103 was chosen as the sample to be used throughout the investigation. The certificate of analysis provided with this standard indicates that Cu and Zn are the primary constituents of the bulk material and account for 59.27 and 35.72 wt % of the sample respectively. The sample also contains minor amounts of Pb, Fe, Sn, Ni and P which were not quantitated in this investigation because of the negligibly small peaks and spectral interferences that were expected. The sample was cylindrical and measured 3.2 cm in diameter and 2.0 cm thick. The sample surface was flat and highly polished. The surface was prepared by initial rough polishing with 600-grit SiC paper and then chemically polishing with a slurry of Fe_2O_3 in a water solution of CrO_3 , on microcloth. The final surface finishing was applied with $1/4\text{-}\mu\text{m}$ diamond paste. After polishing, the sample was stored under He to minimize surface oxidation before sputtering.

The sample was sputtered using a 6-jet glow discharge source (Atomsource, Analyte Corp., Medford, Oregon) which is shown in fig. 1. The source sputters a region that is approximately 1 cm in diameter and produces petal shaped craters around a circle where the 6 gas jets strike the sample surface during the sputtering process as shown in fig. 2. A physical description of the source and its

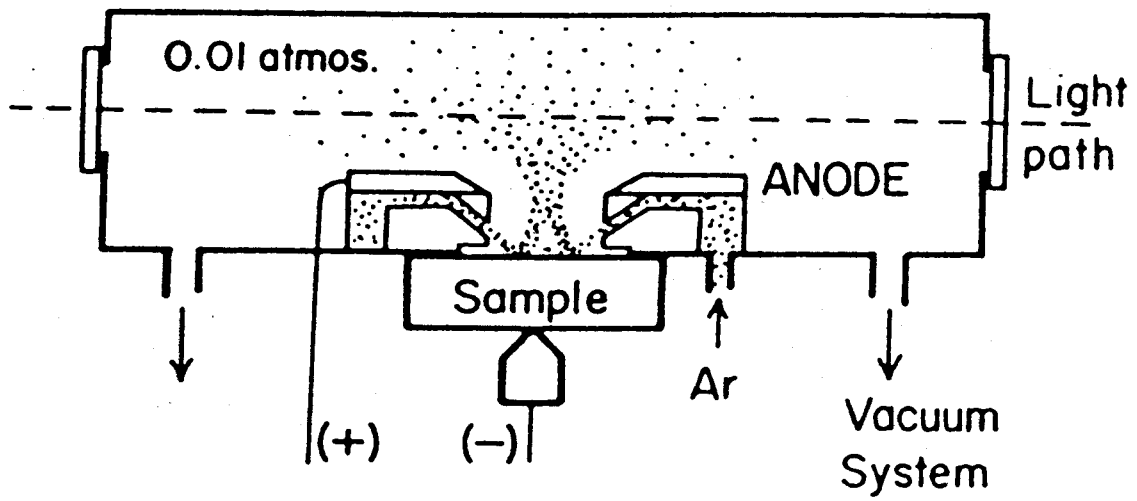


Figure 1. Side view schematic of gas-jet enhanced sputtering atomizer.

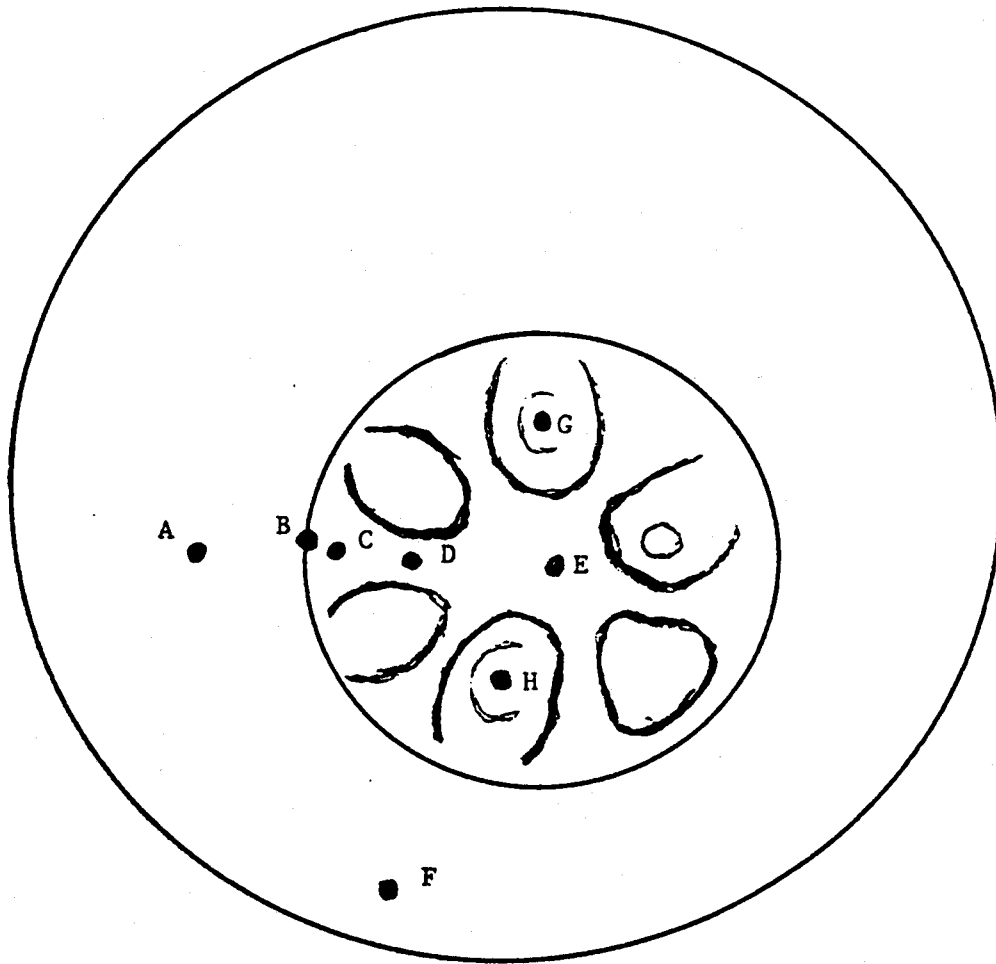


Figure 2. Locations where depth profile data were collected.

operation is presented elsewhere⁽²⁾. The sample was sputtered for a period of 1 minute while maintaining a pressure of 8 torr in the atomization chamber. An applied voltage of 424 V was used producing a current of 60 mA. High purity Ar was used during the sputtering phase of the experiment. The impurities in the Ar are listed by the manufacturer as being O₂ < 5 ppm and H₂O < 3 ppm.

Data collection was done on a Surface Sciences SSX 100 X-ray Photoelectron Spectrometer. The instrument was equipped with an Ar⁺ gun which was used to etch away surface atoms, thereby exposing successive underlying atomic layers for analysis. Depth profiling was done using a generally accepted procedure⁽¹⁰⁾ which consists of alternating data collection and Ar⁺ etch cycles. Data collection cycles consisted of scanning over each of the specified elemental photoelectron emission lines in turn. Scan ranges were chosen so that the spectral lines occurred near the center of the scan range. The entire peak was always contained within the chosen range so that sufficient background on either side of the peak was available to allow good peak fitting. Examples of O, Cu and Zn spectral peaks collected from one of the deposit locations (location C) are presented in fig. 3.

High purity Cu, Zn, and CuO powder were used as standards to determine the instrument response functions used to quantitate the elements Cu, Zn and O. The CuO was measured in the form of a pressed pellet and was lightly

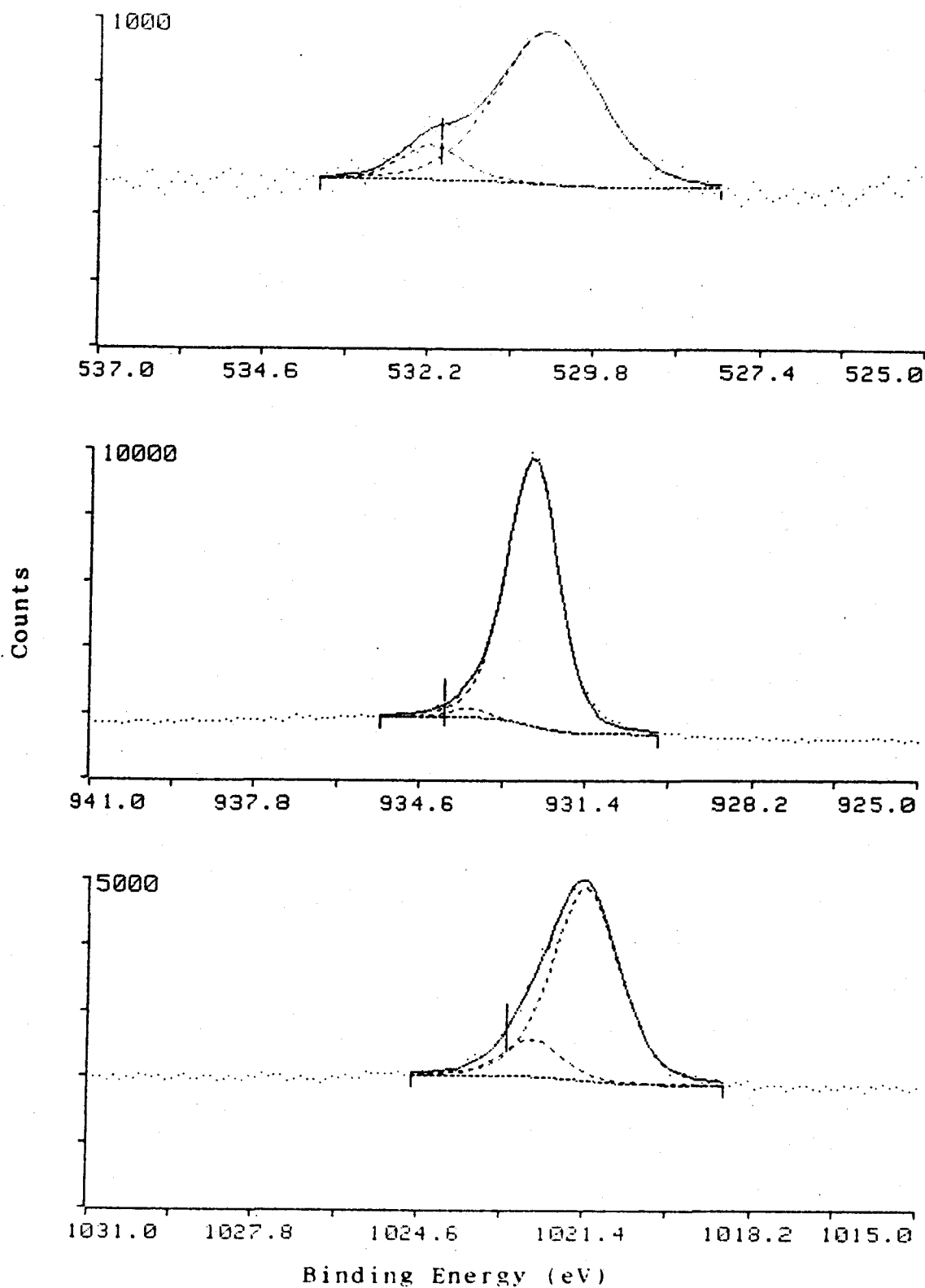


Figure 3. Examples of spectral peaks (binding energy vs. counts) collected at location C after 40 s etch time. (A), O1s, (B), Cu2p3 and (C), Zn2p3. Dashed lines show peaks fitted to data.

etched in the spectrometer to remove adsorbed gases. The instrument response functions were then used in conjunction with elemental peak areas to calculate Zn/Cu and O/Cu atomic ratios using the procedure outlined in the Theory section of this thesis. Calibration of the instrument binding energy scale was done according to the instrument manufacturer's instructions. High purity Au and Cu sheet were used to calibrate the binding energy scale. The binding energy values for metallic Cu and Zn measured during the determination of the instrument response function were 932.4 and 1021.4 eV respectively. These values are in good agreement with values given in the appendix of reference 10.

The sputtering of sample NBS 1103 in the presence of gas jets resulted in the appearance of 3 distinct types of surface areas. Areas which appeared to be unaffected by the sputtering process remained on the sample surface and are designated "bulk" areas. Depressions appeared in areas of the sample which were subjected to gas jets during sputtering with Ar⁺. These areas are designated "crater" areas. The grain structure of the metal was visible in the craters. Material which was sputtered from the craters was deposited on the sample surface. Deposition of sputtered material occurred in a circle around the circumference of the entire sputtered area and at locations between craters. These deposits appeared as dark areas on the surface and ranged in color from dark blue to black.

Figure 2 indicates pictorially the 8 locations where

depth profile information was collected. Two of these locations were in the bulk material and are designated locations A and F. Three areas where deposition occurred are designated locations B, C, and E. Depth profiles were also collected from 2 of the 6 sputtered craters and one location between craters which did not contain deposits but which was affected by the sputtering process. These locations are designated G, H and D respectively.

At each location one objective was to alternately collect data and etch down through surface layers until the bulk of the material was reached. Since it was difficult to know exactly when the bulk of the material was reached, the depth profile was terminated when the oxygen peak became very small or disappeared and the elemental peak areas approached a constant value for several successive data collection-etch cycles. Data collection was done at locations B, C, E, G and H in 2 or 3 stages, each stage consisting of many data collection-etch cycles. Often, between each stage, several hours elapsed during which time the sample remained in the analyzing chamber of the instrument. During the idle times between stages, even at the high vacuum maintained in the analyzing chamber, ambient gas molecules adsorbed onto the sample surface. The result of this data collection scheme is that there are 2 data points provided for a single etch time, one after the last etch cycle of a particular stage and one before the first etch cycle of the next stage. The O/Cu ratio for one of

these 2 data points (the one for the subsequent data collection stage) is slightly higher than the other. In figure 7 (A), the calculated O/Cu atomic ratio data provides a good example of the above. At etch times of 90 and 270 s there are 2 data points given and the point collected at the beginning of the next data collection stage indicates a higher O/Cu ratio. Both Cu and Zn binding energies, as illustrated in figure 7 (B), also appeared to be affected slightly by the addition of adsorbed ambient oxygen to the surface which occurred during these idle times.

The electron spectrometer was equipped with an Al anode X-ray source and a focusing monochromator to select the $K\alpha$ emission line of the source. The X-ray source was operated with a potential difference between anode and cathode of 10 kV. The focusing monochromator was capable of providing an X-ray beam spot size on the sample which ranged from 150 to 1000 microns in diameter. An X-ray spot size of 150 μm was used except during the analysis of the bulk material at point A, when a 300- μm spot size was used.

Research grade Ar gas, with a minimum purity of 99.9995%, was used to produce the Ar^+ etching beam. Ar ions were accelerated through a potential difference of 5 kV and directed onto the target with a 1-mm diameter spot size. An etch rate of 1 $\text{\AA} \text{ s}^{-1}$ was measured using a standard composed of a layer of SiO_2 of known thickness on a Si substrate. Etch rate measurements were made using a 2-mm X 2-mm ion beam spot size. Thus, the etch rate for SiO_2 using a 1-mm diameter spot size was about 5 $\text{\AA} \text{ s}^{-1}$.

RESULTS AND DISCUSSION

Peak binding energy and peak area were extracted from the elemental spectra by curve fitting the individual peaks to Gaussian shapes using the peak fitting software furnished with the instrument. Peak area is proportional to the number density of the atoms producing the peak, according to the relationships discussed previously in the Theory section. Peak binding energy indicates the electronic environment of the atoms producing the peak. Thus, both atomic ratio and chemical state information were acquired for each of the locations investigated.

Bulk Material.

Measurements of the bulk material were made in order to provide a baseline from which to assess changes resulting from the sputtering process. Figure 4 presents the depth profile data for bulk material locations A and F in the form of graphs of atomic ratio (Zn/Cu and O/Cu) vs. etch time. The top profile, at location A, represents an initial data collection cycle and a data collection cycle after each of 9 subsequent 15-s etch cycles. Thus, a total of 135 s of etch time were used at this location. The depth profile in figure 4 (B), at location F, was done in a similar manner except that 39 20-s etch cycles were used for a total etch time of 780 seconds. Surface oxidation, resulting from the exposure of the sample to air, was removed with 600 grit SiC paper prior to the analysis at location F. This oxidation

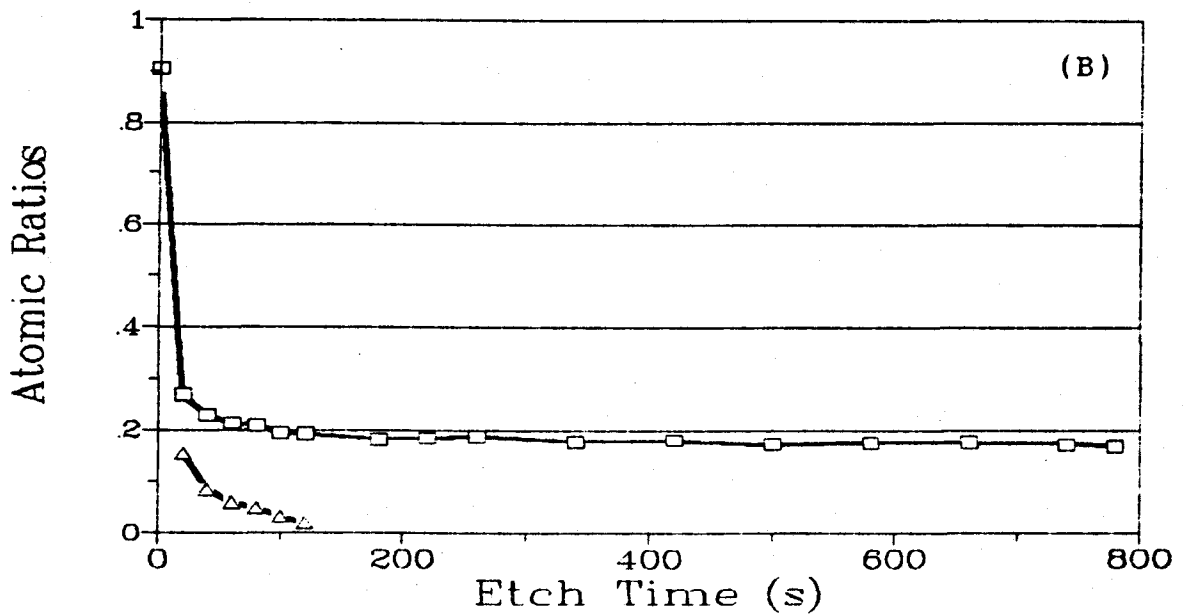
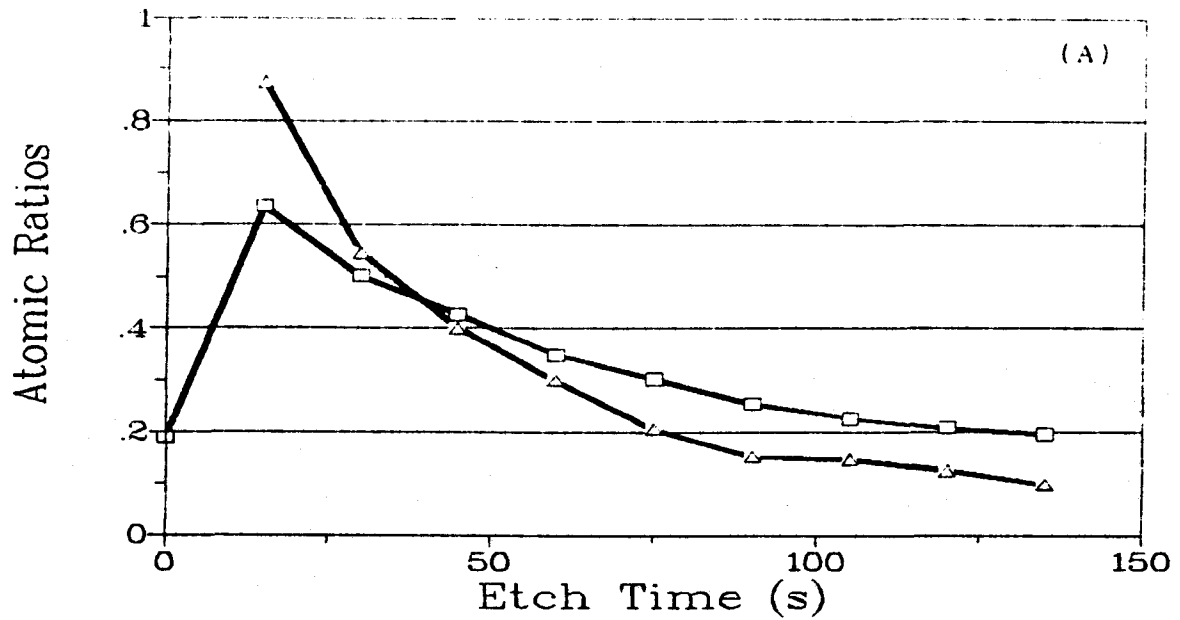


Figure 4. Calculated atomic ratios for locations A and F. Location A (A) and location F (cleaned) (B). (□) Zn/Cu and (△) O/Cu.

removal step was not done at location A.

O/Cu atomic ratios are high (off scale, 3.28 at location A and 2.32 at location F) on the very surface of the sample prior to the first etch (etch time 0 s.) and rapidly decrease with increasing etch time. This observation is consistent with the view of a surface having up to several adsorbed atomic layers of ambient gasses such as O_2 , CO_2 or H_2O which remain adherent even under vacuum. As might be expected the O/Cu atomic ratio at the surface is slightly lower at location F than at location A; the surface at location F had been polished to remove oxides, just before the measurement, while the surface at location A had not. The rate of O/Cu decrease is also faster at location F. After a 40 s etch time the O/Cu ratio at location F is less than 0.2, while an etch time of more than 75 s is required to cause the O/Cu ratio to decrease to less than 0.2 at location A. The longer etch time required to remove oxygen contamination at location A could be attributed to the formation of a surface oxide layer which would be more difficult to remove than a layer of adsorbed gas molecules. The general shape of the O/Cu atomic ratio depth profile is the same for both locations A and F.

After the first etch cycle the general shape of the Zn/Cu depth profile is also the same for both locations A and F. After only a relatively short etch time the measured Zn/Cu atomic ratios are far below the known value for the bulk material. The Zn/Cu atomic ratio calculated from the

certificate of analysis is 0.589. The measured Zn/Cu atomic ratio at the end of the etch times for location A is 0.20 (and still slowly decreasing) and for location F is 0.17. This large difference in atomic ratios between the known bulk value and the value measured after several etch cycles can be quantitatively attributed to the large difference in relative sputtering yields of the elements Zn and Cu under Ar⁺ bombardment. For 5-kV Ar⁺, sputtering yields (atoms/ion) of 13.9 for Zn and 5.1 for Cu have been reported in the literature⁽⁵⁾.

A simple model which predicts surface composition after ion bombardment, from known bulk composition and sputtering yields, has been proposed by Shimizu et al.⁽¹⁵⁾. This model predicts a decrease in the number density of the component with the higher sputtering yield and a concomitant increase in the number density of the lower sputtering yield component until a steady state is reached. The following relationship at steady state is postulated in reference 15:

$$\frac{S_1}{S_2} = \frac{Y_2 B_1}{Y_1 B_2}$$

where the subscripts refer to components 1 and 2, and S refers to the number density at the surface, B the number density in the bulk, and Y the sputtering yield respectively. This model predicts a Zn/Cu atomic ratio of 0.22 for the steady state surface of the sample after etching with 5-kV Ar⁺. This value is in reasonable agreement with the measured steady state values at points A

and F and supports the conclusion that the etching or sputtering of a sample, whose constituents have varying sputtering yields, will result in a change of surface composition. This conclusion has been reached by other workers⁽⁷⁾.

Graphs of peak binding energy vs. etch time for the elements Zn, Cu and O at the bulk locations are shown in figures 5 and 6. These graphs provide information about the sample surface with regard to the chemical environment of the atomic species. When taken in conjunction with the atomic ratios already presented, a fairly complete picture of the surface can be constructed.

Oxygen is removed from the surface with increasing etch time. Therefore the binding energy values, at longer etch times for oxygen show a larger spread as the peaks become noisier. The Zn/Cu ratio, on the other hand, approaches a steady state value wherein both elements retain significant peak areas. The variability of the binding energy values for the elements Cu and Zn is much smaller. Comparison of binding energy values at the two bulk locations indicates that the surfaces at these locations are different. At location A it was necessary to use two peaks in order to adequately fit the observed oxygen data, in contrast to the single peak at location F. One of these two peaks at location A (data not shown) was much smaller and indistinct from the larger peak except when fitting the data from the last few data collection cycles. For the last few data

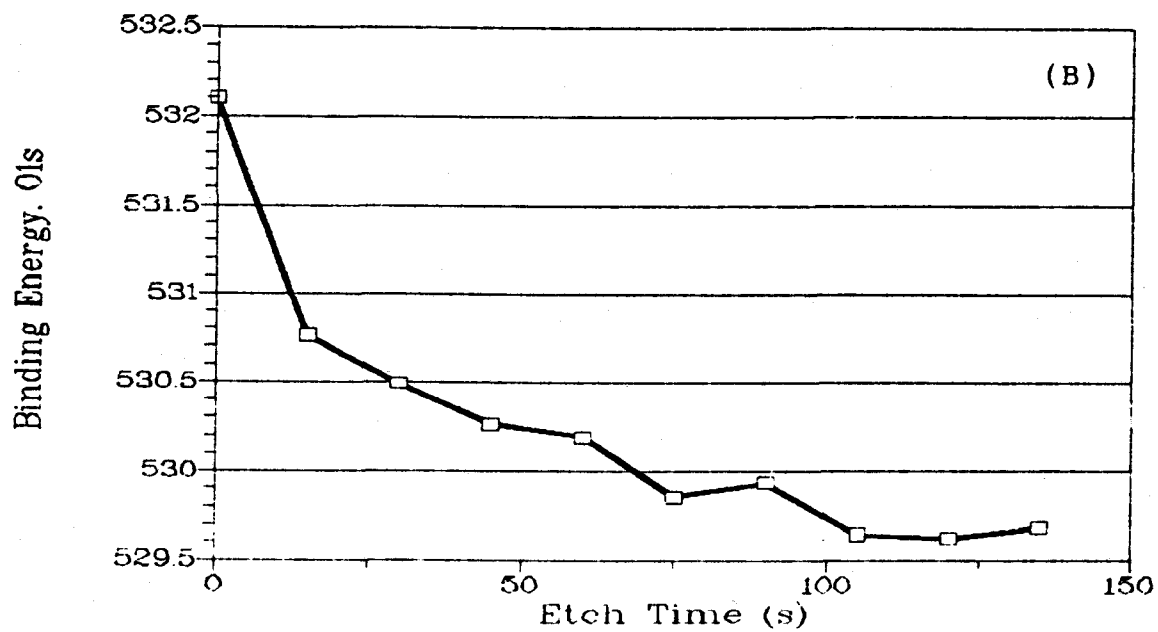
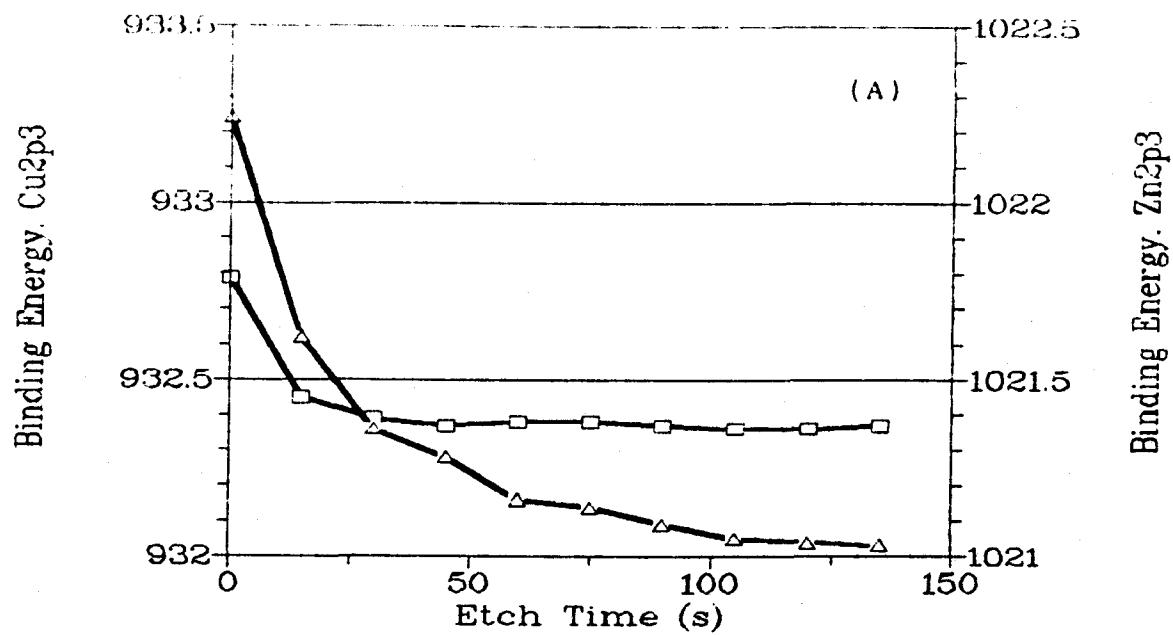


Figure 5. Measured binding energies at location A. (A), Cu(\square) and Zn(\triangle). (B), O(\square).

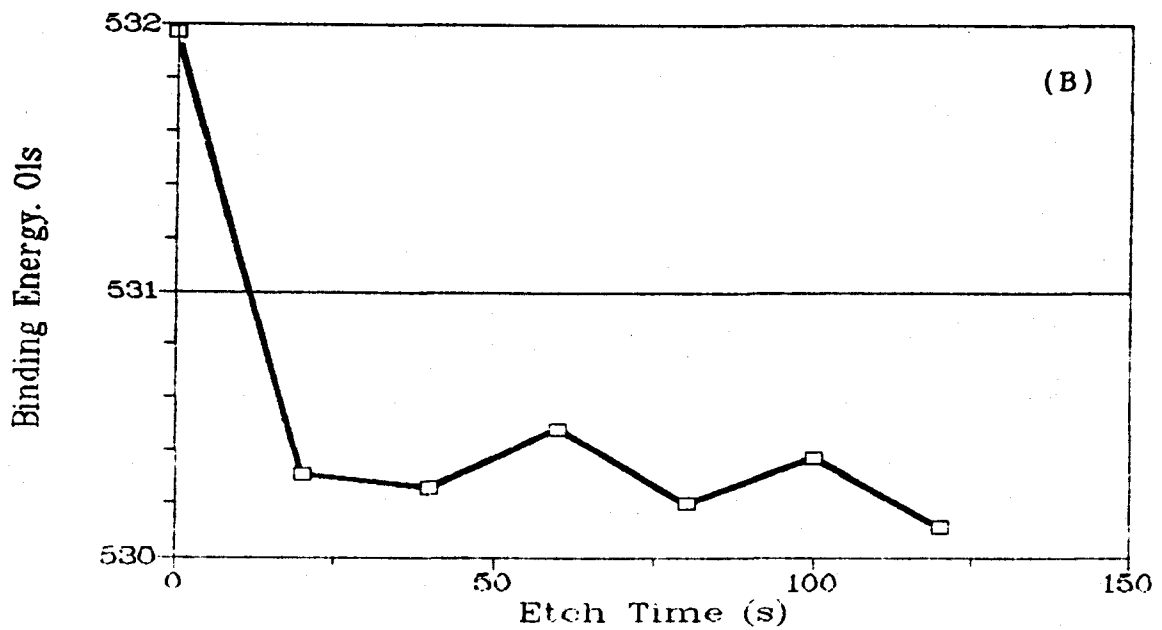
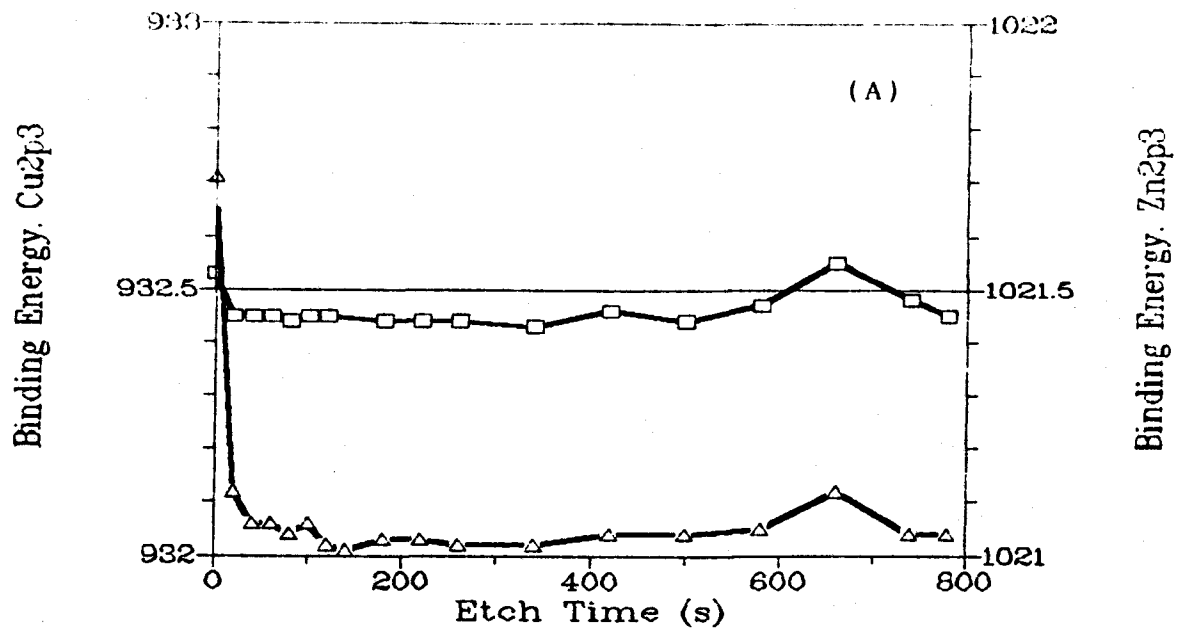


Figure 6. Measured binding energies at location F. (A), Cu(□) and Zn(Δ). (B), O(□).

collection cycles the smaller peak had a binding energy near 531.3 eV. The necessity to use two peaks to fit the data indicates that oxygen may be present at location A in two distinct binding states. The single peak at location F, midway in binding energy between the two peaks at location A, indicates that the small amount of oxygen left on the surface after about 50 s etch time is in a binding state that is midway between the two states at location A. The binding energies of the elements O and Zn show substantial decreases from the higher values at 0 s etch time to the lower values associated with the bulk material. This decrease in binding energy occurs at both bulk locations, but occurs substantially faster at the cleaned location. Only 20 to 40 s of etch time are required to remove any non-bulk species at the cleaned location. Approximately 50 to 60 s of etch time are required to remove non-bulk species at the location that was not cleaned. Reactions at the surface between oxygen bearing species and bulk atoms have proceeded to a greater extent at the uncleaned location, as would be expected. Further evidence for a relatively unreacted surface at the cleaned bulk location is provided by the binding energy vs. etch time graphs for the element Cu.

At the uncleaned location, the binding energy for Cu decreases with increasing etch time. This would be expected if the atoms of Cu were closely associated with those of O, an electronegative element. According to the Charge-Potential model discussed previously in the theory section,

a decrease in electron density around an atom results in an increase in binding energy. At the cleaned bulk location the Cu binding energy remains virtually constant from 0 s etch time until completion of the analysis at that location. At this location it appears that there is no close association between Cu and O. The graphs of Zn and O binding energy have shapes which parallel each other, providing additional evidence that these two elements are closely associated with each other in the surface deposits. Other published research⁽⁷⁾ indicates that the elements Zn and O are removed together during etching; neither element is selectively etched over the other when the two are present.

The picture of the bulk surface then is one in which the elements O and Zn are closely associated with one another in a thin layer. Depth profiling shows that any corrosion products, which might be due to reactions of Zn and Cu with surface oxygen bearing species, are quickly removed during etching. In particular, the O/Cu atomic ratio decreases continuously from a very high value at etch time 0 s to a low value as the bulk of the material is reached. The composition of the bulk surface after etching with 5-kV Ar⁺ is changed substantially from that of the bulk material. The surface is enriched in the element Cu, the component with the lower sputtering yield, according to a simple model which relates bulk composition, sputtering yield and surface composition. The measured surface composition is close to that predicted by the model.

Surface Deposits.

Three areas which appeared to contain surface deposits were analyzed. These areas are designated locations B, C and E on figure 2. Location B was part of a 1-mm wide darkly colored ring around the entire circumference of the area exposed to the sputtering environment. Location C was a darkly colored area between two of the sputtered craters toward the outside of the sputtered area. Location E was also darkly colored and was near the center of the sputtered area.

The atomic ratio depth profiles of these 3 locations, presented as figures 7, 8 and 9, have a common feature which distinguishes them from those of the bulk material. Both bulk locations (figure 4 (A) and (B)) are characterized by a rapidly decreasing Zn/Cu ratio and near attainment of the predicted equilibrium value of 0.22 after only about 100 sec of etch time. Both of these bulk locations exhibit a high initial O/Cu ratio which decreases rapidly with increasing etch time. In contrast, the Zn/Cu and O/Cu ratios at the deposit locations in figures 4-6 show an increase with etch time, rising to a peak, and then falling off again, two of them eventually reaching near the predicted equilibrium value of 0.22. The rise in O/Cu atomic ratio was unexpected. A possible source of O is the Ar gas used during the sputtering process. As previously noted this gas contains less than 5 ppm O₂. Another source of O could be the gasses adsorbed on the sample surface. The Zn/Cu ratios

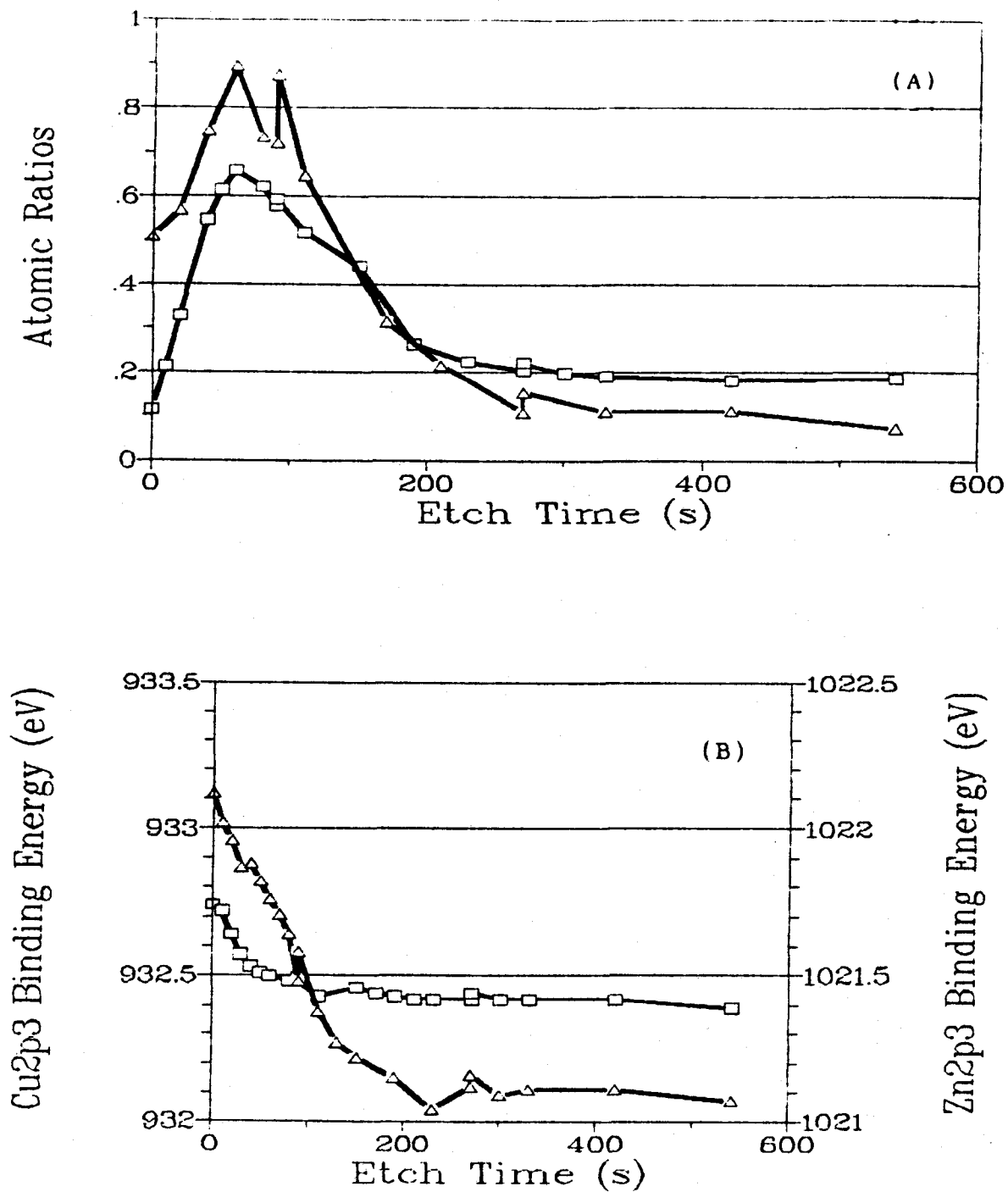


Figure 7. Calculated atomic ratios and measured binding energies at location B. (A), atomic ratios, Zn/Cu(□) and O/Cu(Δ). (B), binding energies, Cu(□) and Zn(Δ).

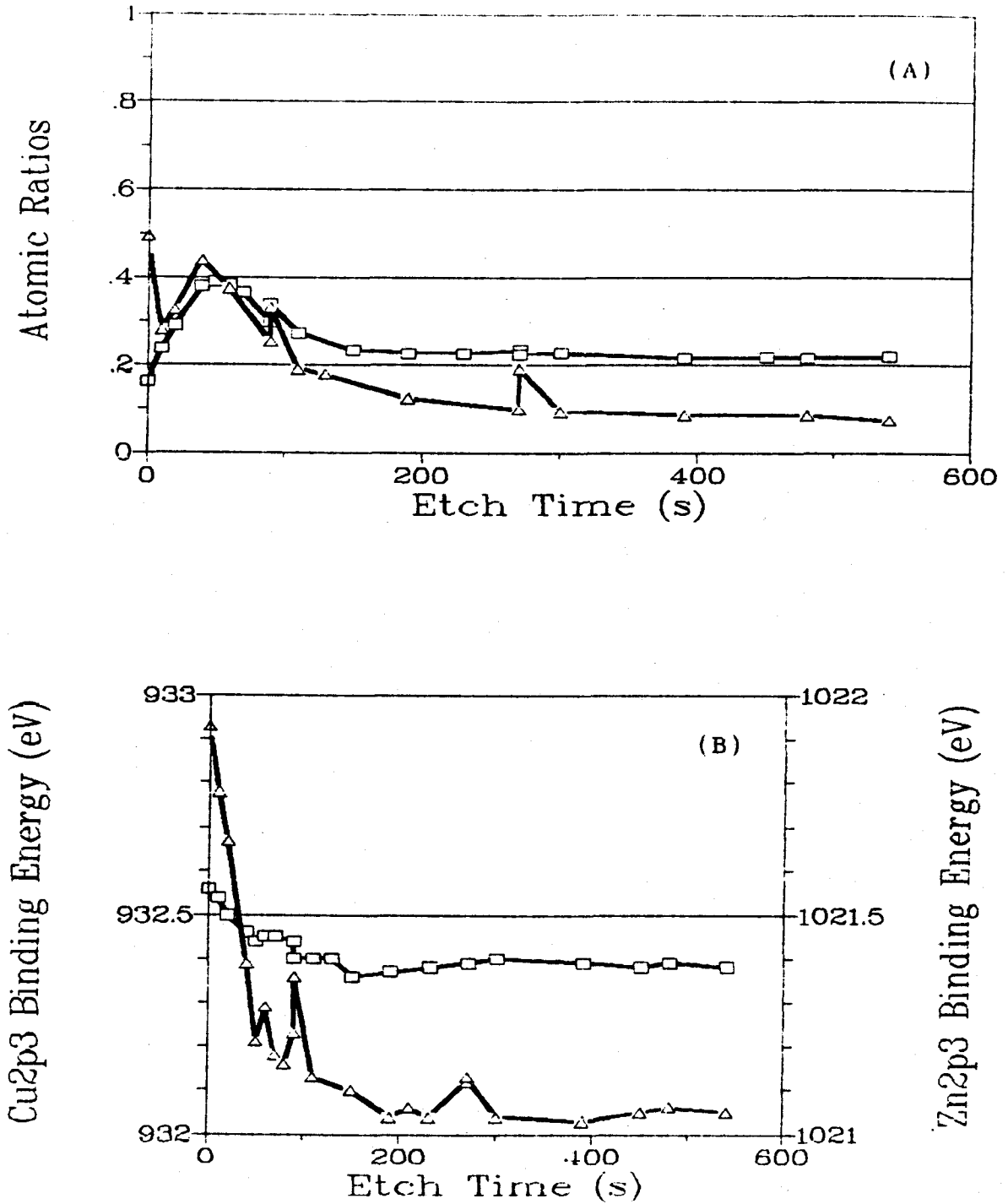


Figure 8. Calculated atomic ratios and measured binding energies at location C. (A), atomic ratios, Zn/Cu(□) and O/Cu(△). (B), binding energies, Cu(□) and Zn(△).

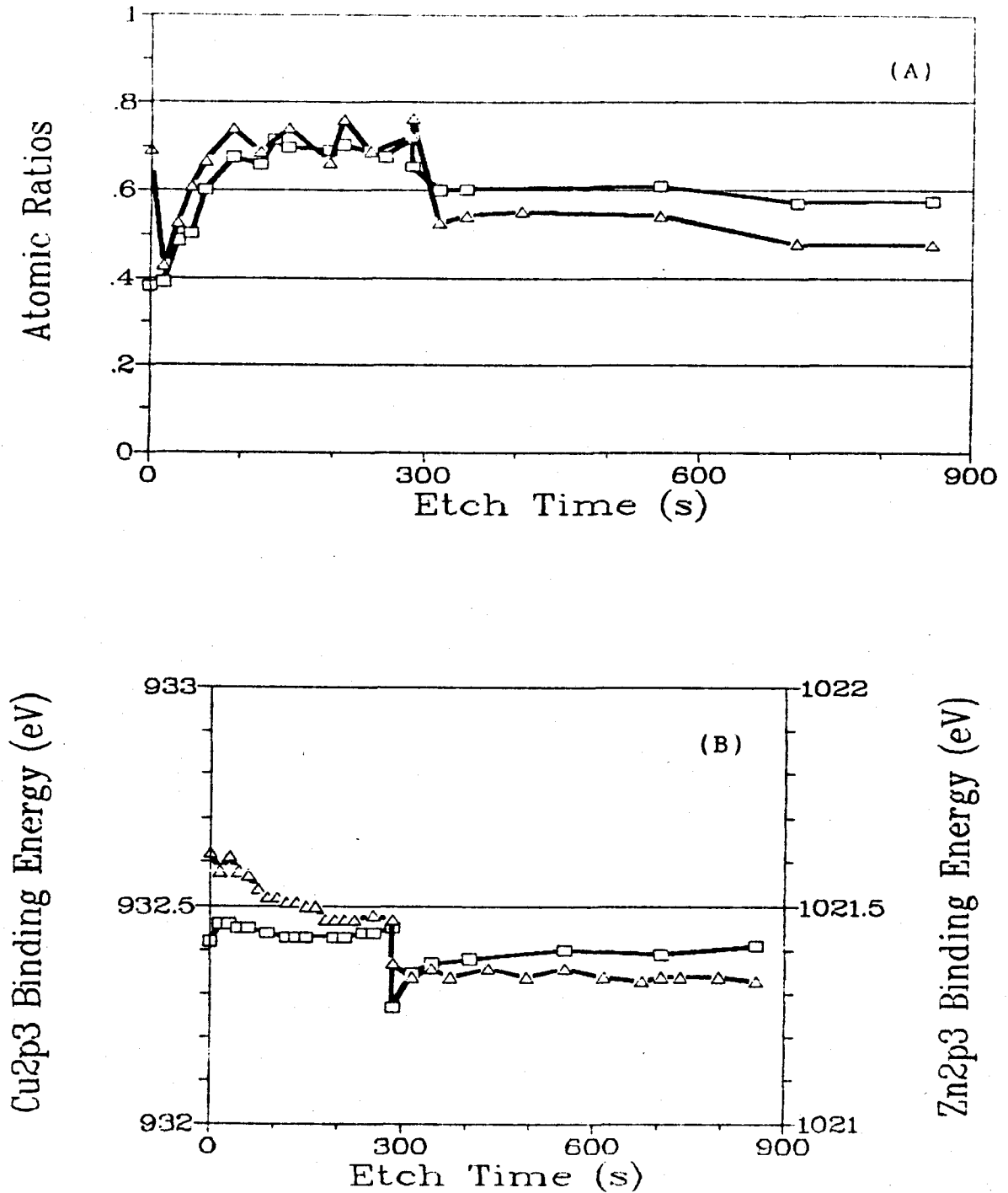


Figure 9. Calculated atomic ratios and measured binding energies at location E. (A), atomic ratios, Zn/Cu(□) and O/Cu(Δ). (B), binding energies, Cu(□) and Zn(Δ).

at locations B, C and E all start out low with respect to the bulk Zn/Cu ratio of 0.589 and rise with increasing etch time to peaks of 0.63, 0.39 and 0.71 respectively.

The Zn/Cu ratio at location B, figure 7 (A), rises to a value which is relatively close to the bulk Zn/Cu ratio. It is therefore plausible that at location B, after an etch time of about 60 s, the surface deposit has been etched away and the bulk of the metal has been reached. At etch times prior to 60 s, the atomic ratios measured are those of the deposit, and at etch times greater than 60 s the atomic ratios measured are those of the bulk metal. The O/Cu ratio also rises and peaks at the same time that the Zn/Cu ratio peaks. The fact that the O/Cu depth profile closely follows the Zn/Cu depth profile indicates that O and Zn are closely associated in the deposit. The binding energy depth profiles for Zn and Cu at location B, figure 7 (B), do indicate that Zn is the more highly oxidized of the two species because of the much larger decrease in the binding energy of Zn. The Cu binding energy changes from 932.74 eV at the surface to 932.39 eV at the end of the etch time, a decrease of 0.35 eV. In contrast, the Zn binding energy changes from 1022.12 eV at the surface to 1021.08 eV at the end of the etch time, a drop of 1.04 eV.

The oxygen binding energy change at location B (not shown) is similar to that of the bulk locations. The principal oxygen peak showed a binding energy change from 531.76 at 0 s etch time to a value of 529.5 after an etch

time of 250 s, a decrease of 2.3 eV. It was also necessary to use 2 peaks at location B to fit the oxygen data, as were used at bulk location A. As at location A, the use of 2 peaks indicates the possibility of 2 distinct binding states.

The depth profiles at location C, figure 8, are similar in many respects to those at location B. The Zn/Cu atomic ratio rises from a value below 0.2 to a peak, and then drops off again, leveling off and remaining near the predicted equilibrium value of 0.22. The peak in the Zn/Cu ratio occurs at about the same etch time as at location B, but only reaches a value of 0.39 before starting to drop again. If the peak in the depth profile indicates that the bulk of the metal has been reached, as it seemed to at location B, then the bulk metal Zn/Cu ratio is low at this location. It is possible that some selective sputtering had occurred before the deposit was laid down resulting in a lower metal surface Zn/Cu ratio over which the deposit formed. This seems reasonable since location C is closer to the center of the sputtered region while location B is at the edge.

At both locations B and C the surface deposit portion of the depth profile can be explained in terms of the sputtering ratios of Zn and Cu. The measured atomic ratios indicate that the surface of the deposit is rich in Cu, but the deposit becomes richer in Zn with depth. The uppermost layers of a surface deposit should be a reflection of the conditions at the end of the sputtering time in the sense

that the atoms at the top of the deposit were laid down last. Also, the atoms nearest the bulk metal should reflect the conditions at the very beginning of the sputtering time. At the end of the 1 minute sputtering time, since the deposit is richer in Cu than the bulk composition, the atomic vapor being removed from the nearby crater should also have been richer in Cu. This is consistent with the fact that Zn is sputtered preferentially initially, leaving a bulk which is rich in Cu from which the atomic vapor is produced. At the beginning of the sputtering time Zn would be preferentially sputtered producing a vapor rich in Zn to be deposited closest to the bulk metal. Thus, the deposit nearest the bulk would be richer in Zn, and the deposit farthest from the bulk metal, that is, the surface of the deposit, would be richer in Cu. The result of this selective sputtering process is shown graphically in figure 10.

At location E, figure 9 (A), the Zn/Cu ratio rises to a peak of 0.71 and remains high for a relatively long period of etch time, about 200 s, and then gradually begins to taper off, never decreasing to the equilibrium expected value of 0.22. After a total etch time of 855 s, the Zn/Cu atomic ratio has only decreased to 0.58. The O/Cu ratio starts out at 0 s etch time at a relatively high value, dropping suddenly to just below 0.5 after 1 etch cycle, probably due to adsorbed ambient gasses being quickly removed. The O/Cu ratio then increases in a fashion

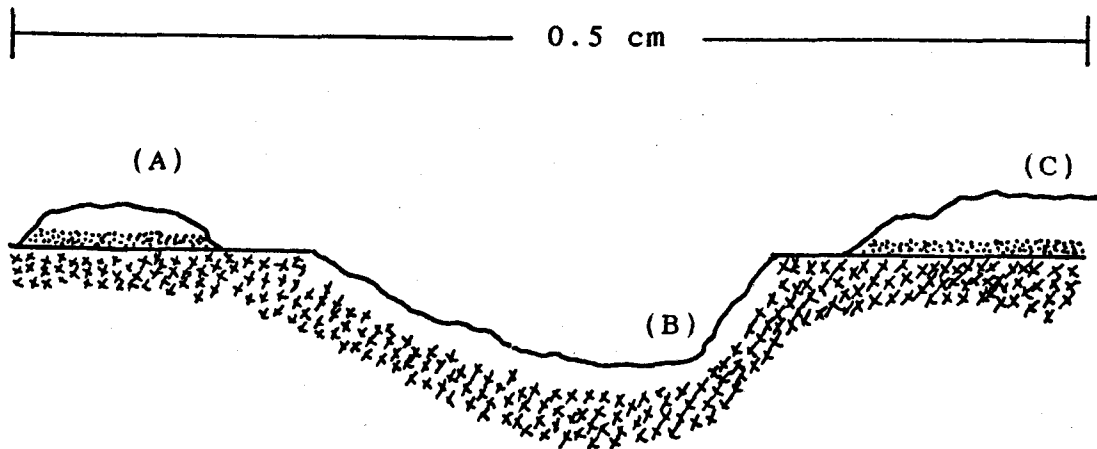


Figure 10. Cross sectional diagram indicating the changes to the sample surface resulting from gas-jet enhanced sputtering by the Atomsources. (A), surface deposit around circumference of sputtered area, (B), crater resulting from ion bombardment, and (C), deposit at center of sample. [···], Zn rich zones, [××], Cu rich zones and [—], bulk zones.

parallel to that of the Zn/Cu ratio to a maximum value of 0.76 and then begins to drop. The decrease is quick at first and then begins to taper off with the O/Cu ratio falling only to 0.48. It is apparent that at this location the bulk of the metal was not reached by the last etch cycle. Had it been reached, the Zn/Cu ratio would have dropped to a value near 0.22 and the Zn and O binding energies would have dropped to values near 1021.1 eV and 529.6 eV respectively. The deposit at the center of the sputtered area appears to be either thick or tenacious, or both.

Crater Areas.

Three areas which are designated crater locations were analyzed. Two of these locations were inside craters produced by the 6 gas jets of the Atomsources. These areas are designated locations G and H on figure 2. The third area is located between two of the craters but appears visually to have been subjected to sputtering. This area is designated location D on figure 2. Microscopically, the inside of both craters and the area between the craters, location D, had a metallic appearance. Additionally, in the two crater locations, the grain structure of the metal was visible. The grain structure of the metal was not visible in any of the other locations analyzed.

The atomic ratio depth profiles at the 3 crater locations, figures 11, 12 and 13 are distinct from those of

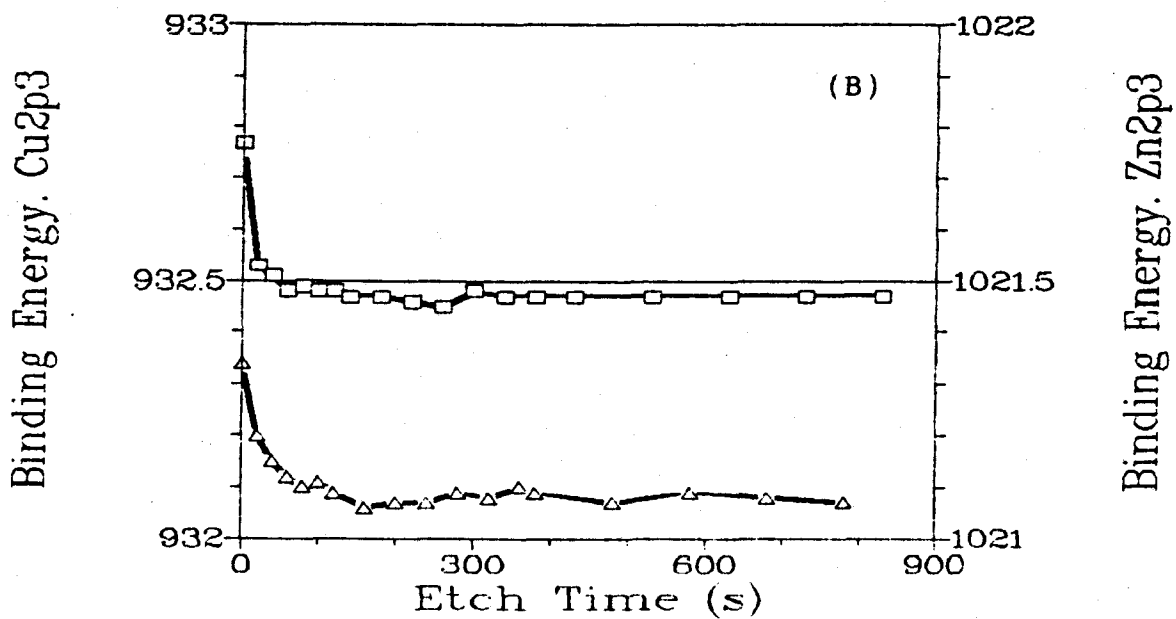
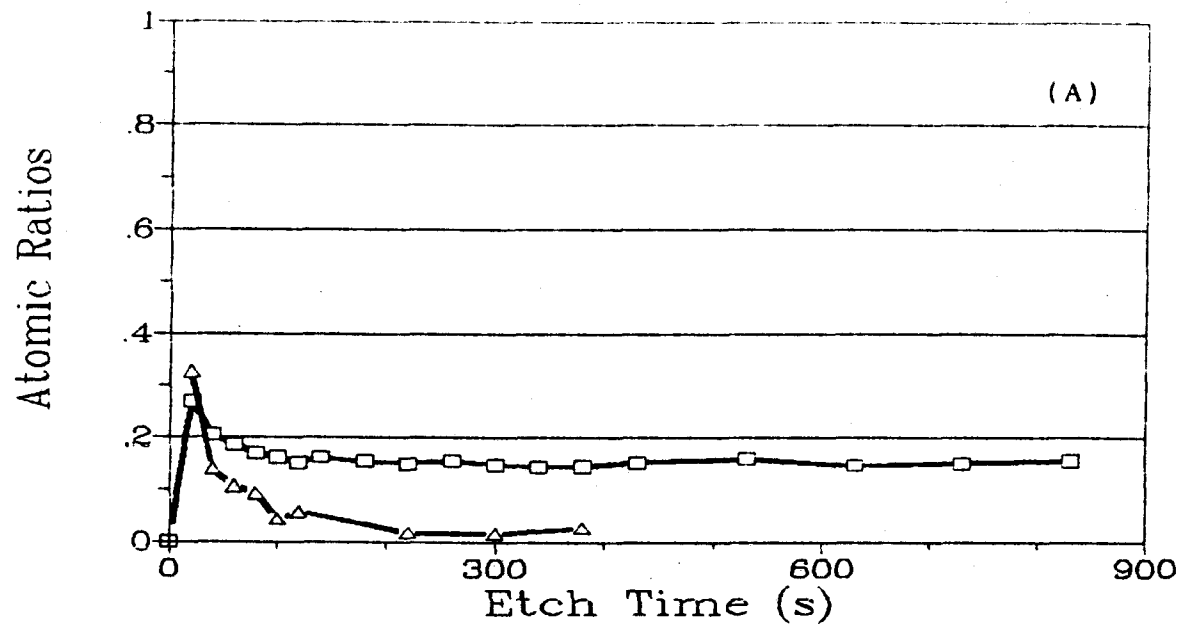


Figure 11. Calculated atomic ratios and measured binding energies at location G. (A), atomic ratios, Zn/Cu(□) and O/Cu(Δ). (B), binding energies, Cu(□) and Zn(Δ).

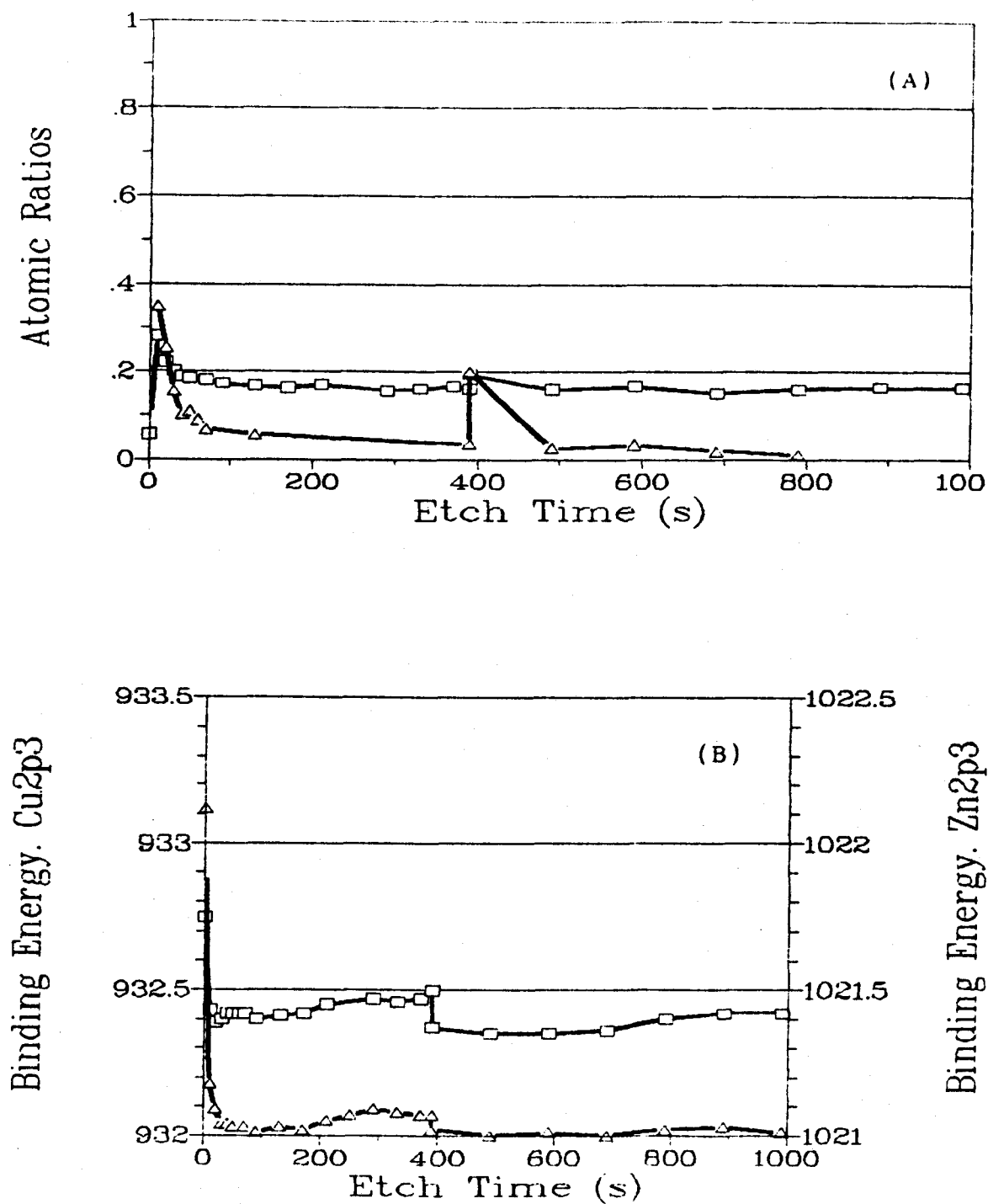


Figure 12. Calculated atomic ratios and measured binding energies at location H. (A), atomic ratios, Zn/Cu(\square) and O/Cu(Δ). (B), binding energies, Cu(\square) and Zn(Δ).

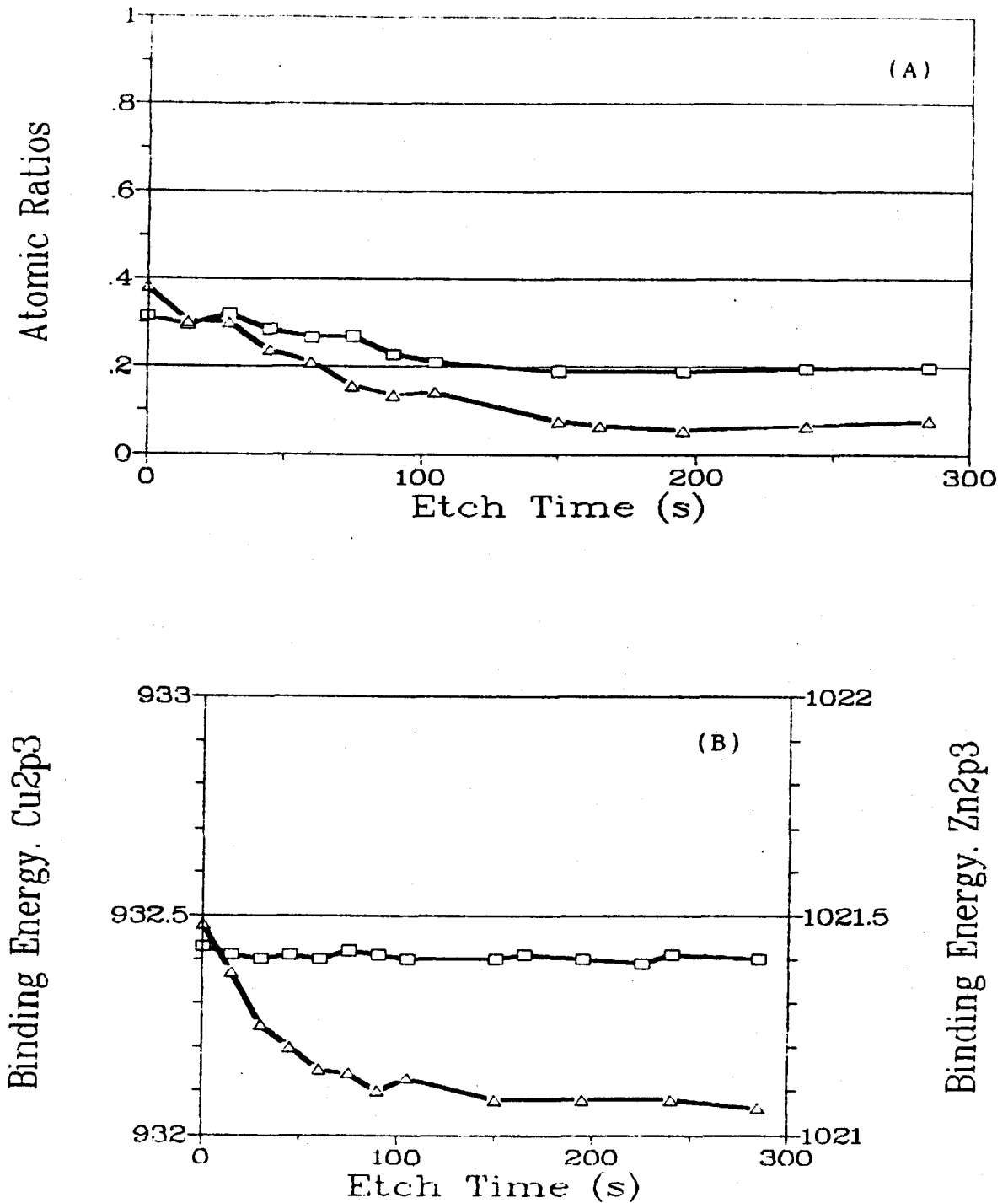


Figure 13. Calculated atomic ratios and measured binding energies at location D. (A), atomic ratios, Zn/Cu(□) and O/Cu(Δ). (B), binding energies, Cu(□) and Zn(Δ).

the bulk and deposit locations. The depth profiles at locations G, H and D do not exhibit the pronounced peak in Zn/Cu and O/Cu atomic ratios with etch time as did the depth profiles at the deposit locations. Thus it would appear that there has been no redeposition of sputtered material back into the craters, as was found at the deposit locations.

Both Zn/Cu and O/Cu atomic ratio depth profiles at locations G and H do have shapes that are similar to those measured at bulk location A, the uncleaned location. The O/Cu atomic ratio depth profiles start at a very high value (off scale, 3.72 at location G and 1.60 at location H) on the surface and decrease rapidly to low values, just as they did at the bulk locations. The Zn/Cu atomic ratios at locations G and H start low at the very surface and after 1 etch cycle rise to a peak. Subsequent etching causes the Zn/Cu ratios to decrease steadily to values near the predicted equilibrium value of 0.22. The difference between the bulk location A and the two crater locations G and H lies in the maximum values for the Zn/Cu ratios that are attained. After the initial etch cycle at the bulk location the Zn/Cu ratio reaches a value of 0.64, close to the known bulk value of 0.589. The maximum values attained at the crater locations, G and H, however are only 0.27 and 0.28 respectively. The fact that the measured Zn/Cu ratios in the craters is substantially lower than that measured for the bulk location indicates selective sputtering has occurred. The craters have been subject to energetic Ar⁺

bombardment by the Atomsorce which caused selective sputtering due to the great difference in the sputtering yield of Zn and Cu. The craters were thus enriched in Cu and depleted in Zn. Only about 100 seconds of etch time are required to attain the Zn/Cu equilibrium value at locations G and H. Final values of 0.16, well below the equilibrium value, were observed for both locations and are the lowest measured at any of the 8 locations. These low values may be due to the fact that the Zn/Cu atomic ratios were low to begin with on the surface as a result of sputtering by the Atomsorce. Since the equilibrium surface atomic ratio is dependent on the bulk atomic ratio, if sputtering in the Atomsorce had caused a decrease in the Zn/Cu atomic ratio to a substantial enough depth, then the measured equilibrium surface atomic ratio would also be smaller.

After the first etch cycle, the shape of the atomic ratio profiles at location D between the craters is similar to those of bulk location A and crater locations G and H. The Zn/Cu atomic ratio at location D also starts out at a rather low value with respect to the bulk, 0.34, and decreases to near the expected equilibrium value of 0.22 after approximately 100 seconds of etch time. The low initial Zn/Cu value can be attributed to selective sputtering in this location as it was in the other two crater locations. The O/Cu atomic ratio at location D starts out at a relatively low value, 0.38, however, in comparison to the other two crater locations which had

initial O/Cu ratios of 3.72 and 1.62. There are apparently minimal amounts of adsorbed ambient gasses at this location, possibly due to the fact that the analysis at location D was accomplished before the analyses at the other crater locations. The sample was exposed to the atmosphere between the analyses at locations D and G and H.

The binding energy profiles for all locations G, H and D are consistent with the measured atomic ratio profiles. The general trends exhibited by the profiles are from a higher binding energy initially to a lower binding energy characteristic of metallic Cu and Zn in the sample bulk. Adsorbed ambient electron withdrawing species, such as oxygen, on the surface would account for the trend. At both crater locations G and H, Cu and Zn binding energies exhibit the downward trend with etch time. At location D the Zn binding energy exhibits the same downward trend while the Cu binding energy remains virtually constant from the beginning to the end of the analysis. At location D the Zn atoms appear to be associated with the electron withdrawing species on the surface, while the Cu atoms do not. The final binding energies reached for Cu and Zn at the 3 crater locations are very similar to those reached at bulk locations A and F. At locations G and H the final oxygen binding energies were very similar to one another and were near the final binding energy at location F, the cleaned location. At location D the oxygen peak was fitted with 2 peaks, again indicating the possibility that oxygen is

present in two different binding states, as it seems to be at location A. The final binding energies of these peaks at location D are close to those at location A, the uncleaned location.

CONCLUSIONS

Some of the effects that inert gas ion sputtering has on solid surfaces can be understood in the light of observations made during the course of this investigation. Selective sputtering of bulk components helps explain the observed data.

Surface deposits were observed, after sample sputtering, on areas which were not subject to the gas jets during sputtering. The change in composition of surface deposits with depth can be related to the selective sputtering effect. The atomic ratio data indicate that the bulk component with the lowest sputtering yield predominates in the uppermost layers of the deposit, while the high sputtering yield component can be found to a relatively greater extent in the lower layers of the deposit. The low sputtering yield component has the smallest tendency to be sputtered and hence is removed from the bulk to a larger extent at later times during the sputtering. Deposit layers formed at later times during sputtering are therefore enriched in the lower sputtering yield component. The converse is true for the bulk component which has the highest sputtering yield.

Composition data from the sputtered craters, and from an area between the craters, indicates that selective sputtering occurs under the conditions which were used to produce the sample. When compared to the bulk, atomic ratio

data indicate that the crater locations are depleted in the higher sputtering yield component and enriched in the lower sputtering yield component, as would be predicted.

Comparison of atomic ratio data from craters and surface deposits also indicates that redeposition of sputtered material is not occurring inside the craters.

BIBLIOGRAPHY

- (1) C.G.Bruhn and W.W.Harrison, *Anal. Chem.*, 50, 16, (1978)
- (2) H.J.Kim and E.H.Piepmeyer, *Anal. Chem.*, 60, 2040, (1988)
- (3) M.P.Seah, *Thin Solid Films*, 81, 279, (1981)
- (4) N.Laegreid and G.K.Weher, *J. Appl. Phys.*, 32, 365, (1961)
- (5) H.Schirrwitz, *Contrib. to Plasma Phys.*, 2, 188, (1962)
- (6) H.Oechsner, *Appl. Phys.*, 8, 185, (1975)
- (7) R.Kelly, *Nucl. Instr. and Methods*, 149, 553, (1978)
- (8) E.H.Daughtrey, Jr., D.L.Donohue, P.J.Slevin and W.W.Harrison, *Anal. Chem.*, 47, 683, (1975)
- (9) R.Holm and S.Storp, *Physica Scripta*, 16, 442, (1977)
- (10) S.Hofmann, "Practical Surface Analysis by Auger and X-ray Photoelectron Spectroscopy", D.Briggs and M.P.Seah, Eds., John Wiley and Sons, 1987, Chapter 4.
- (11) D.Briggs and J.C.Riviere, "Practical Surface Analysis by Auger and X-ray Photoelectron Spectroscopy", D.Briggs and M.P.Seah, Eds., John Wiley and Sons, 1987, Chapter 3.
- (12) C.J.Powell, "The Physical Basis for Quantitative Analysis by Auger Electron Spectroscopy and X-ray Photoelectron Spectroscopy" in "Quantitative Surface Analysis of Materials", N.S.McIntyre, Ed., American Society for Testing and Materials Special Technical Publication 643, Philadelphia, PA., 1978.
- (13) J.H.Schofield, *J. Elect. Spec. and Related Phenom.*, 8, 129, (1976)
- (14) S.Tanuma, C.J.Powell and D.R.Penn, *Surf. and Interface Anal.*, 17, 911, (1991)
- (15) H.Shimizu, M.Ono and K.Nakayama, *Surf. Sci.*, 36, 817, (1973)

APPENDIX

APPENDIX

The following table lists values of $\lambda_{Cu}/\lambda_{Zn}$ and λ_{Cu}/λ_O calculated according to the method given in reference 14. The quantities required for the calculation are the photoelectron energies, the number of valence electrons in the molecule, the density of the compound and the molecular weight of the compound. The photoelectron energies, given in eV, for Cu, Zn and O used in the calculation are 555, 466 and 956 respectively. The other quantities were varied in accordance with the table to arrive at the given ratio of inelastic mean free paths.

Element or Compound	Molecular Weight (g)	Density (g/cm ³)	Valence Electron #	$\lambda_{Cu}/\lambda_{Zn}$	λ_{Cu}/λ_O
Cu	63.58	8.92	11	1.13	0.677
CuO	79.54	6.5	17	1.13	.675
"	"	6.0	"	1.13	.674
"	"	7.0	"	1.13	.675
"	"	6.5	10	1.13	.675
"	"	"	15	1.13	.675
"	"	"	20	1.13	.673
Zn	65.38	7.14	12	1.13	.676
ZnO	81.37	5.61	18	1.13	.674
"	"	5.0	"	1.13	.673
"	"	6.0	"	1.13	.674
"	"	5.6	12	1.13	.673
"	"	"	15	1.13	.674
"	"	"	20	1.13	.674
CuZnO	144.92	5.0	29	1.13	.673
"	"	5.5	"	1.13	.674
"	"	6.0	"	1.13	.675
"	"	6.5	"	1.13	.675
"	"	7.0	"	1.13	.675
"	"	7.5	"	1.13	.675
"	"	8.0	"	1.13	.675
"	"	8.5	"	1.13	.675
"	"	7.5	20	1.13	.677
"	"	"	27	1.13	.677
"	"	5.0	31	1.13	.673
"	"	9.0	20	1.13	.678